a very interesting result because it indicates that at the clean surface the densities of surface states and recombination centers differ by a factor, but not by orders of magnitude. The same is true for the real germanium surface.[31]

ACKNOWLEDGMENTS

The author would like to express his sincerest thanks to Dr. S. P. Wolsky, Dr. E. J. Zdanuk, and Dr. D. Shooter for their help in designing and operating the ultrahigh vacuum system. Professor H. E. Farnsworth's and Professor J. A. Dillon's assistance during the design of the experimental tube was very much appreciated. I am also indebted to J. Silva for supervising the construction of the tube, to L. Rubin for his help with the electronic equipment, and to W. Gowell and J. Gage for all the glass work. R. Leighton's technical assistance was invaluable.

PHYSICAL REVIEW VOLUME 132, NUMBER 5 1 DECEMBER 1963

Optical Properties of Aluminum

H. EHRENREICH,* H. R. PHILIPP, AND B. SEGALL
General Electric Research Laboratory, Schenectady, New York
(Received 31 July 1963)

The frequency-dependent complex dielectric constant $\epsilon(\omega)=\epsilon_1+i\epsilon_2$ and associated functions are derived in the range 0 to 22 eV by application of the Kramers–Kronig relations to existing reflectance data for clean Al surfaces. The results are quantitatively interpreted in terms of intra- and interband transitions as well as plasma oscillations. The decomposition of $\epsilon(\omega)$ into intra- and interband parts given here is seen to be valid in the presence of electron-electron interactions. Due to these interactions the optical effective mass $m_a=1.5$, deduced from experiment in the free-carrier region, is appreciably larger than that obtained using Segall's band calculations ($m_{ac}\cong 1.15$). The band calculations are extended to higher energies in order to examine the effect of interband transitions for the range of interest. It is found that the only interband transitions which lead to significant structure in $\epsilon_2(\omega)$ are those that occur around W and Σ in the vicinity of K in the Brillouin zone and that these produce a peak near 1.4 eV. These conclusions are in accord with the experimentally determined $\epsilon_2(\omega)$ which exhibits a peak at 1.5 eV and has no further structure at higher energies. The result of a quantitative calculation of the structure in $\epsilon_2(\omega)$ using a fine mesh of points in $\mathbf{k}$ space and an approximate variation of the momentum matrix element with $\mathbf{k}$ is in good agreement with the experimental results with respect to shape but has a magnitude which is somewhat too low. From the known influence of many-electron effects on the intraband contribution to $\epsilon(\omega)$ and a general sum rule, the corresponding effect on interband transitions may be estimated and shown roughly to account for the difference. The derived $\epsilon(\omega)$ indicates the presence of a sharp plasma resonance at $\hbar\omega_p=15.2$ eV, in excellent agreement with the results of characteristic energy loss experiments. It is shown that this resonance may be interpreted either in terms of electrons characterized by the low-frequency optical mass and screened by the interband dielectric constant at ω_p or, since the f sum has been essentially exhausted, in terms of the exact asymptotic formula for ϵ in which all carriers are unscreened and have the free-electron mass.

I. INTRODUCTION

THE properties of Al have been studied quite extensively during the past few years. This interest has resulted from the fact that it has been possible to observe a number of phenomena yielding direct information about the Fermi surface, including its topology, notably the de Haas-van Alphen effect,[1] the magnetoacoustic effect,[2] and cyclotron resonance.[3] Further, the band structure has been shown to be nearly free electron-like by a number of independent calculations,[4–6] the results of which are all mutually consistent. These calculations have been quite successful in yielding a Fermi surface in quantitative agreement with the experimental results, although the nature of the connectivity of the third band arms has yet to be resolved.[7,8]

In this paper we shall discuss in terms of the existing information another type of experiment which yields the optical constants. We shall use an approach similar to that previously shown successful in connection with Ag and Cu.[9] The optical properties principally yield evidence about excited electronic states of the crystals and, in particular, the magnitude of some gaps at

* Present address: The Division of Engineering and Applied Physics, Harvard University, Cambridge, Massachusetts.

[1] E. M. Gunnerson, Phil. Trans. Roy. Soc. London **249A**, 229 (1957); M. G. Priestly, *Proceedings of the Seventh International Conference on Low-Temperature Physics* (University of Toronto Press, 1960), p. 230; W. L. Gordon and K. Larson (private communication).

[2] B. W. Roberts, Phys. Rev. **119**, 1889 (1960); G. Kamm and H. V. Bohm, Phys. Rev. **131**, 111 (1963).

[3] T. W. Moore and F. W. Spong, Phys. Rev. **125**, 846 (1962); **126**, 2261(E) (1962).

[4] V. Heine, Proc. Roy. Soc. (London) **A240**, 361 (1957).

[5] W. A. Harrison, Phys. Rev. **118**, 1182 (1960).

[6] B. Segall, Phys. Rev. **124**, 1797 (1961).

[7] N. W. Ashcroft, Phys. Rev. Letters **3**, 202 (1963).

[8] B. Segall, Phys. Rev. **131**, 121 (1963).

[9] H. Ehrenreich and H. R. Philipp, Phys. Rev. **128**, 1622 (1962).

symmetry points of the Brillouin zone. Because of the essentially free-electron character of the Al band structure, we should expect interband effects to be less important than in Ag and Cu. The plasma frequency should lie at somewhat higher energies because Al is polyvalent.

The optical properties indeed are found to differ appreciably from those of the monovalent metals. The reflectance remains greater than 85% for photon energies as high as about 12 eV. Above this energy it falls off as expected for a free-electron metal near the plasma frequency. As we shall show, interband transitions are significant only near 1.5 eV and are associated with critical points at W and around the Σ axis near K. This degree of simplicity implies that the quantitative aspects of the theory for the optical properties can be pushed rather further than in other metals.

Significant data[10,11] on Al have been available for some time. Most recently some precise ultrahigh vacuum data which cover a substantial part of the spectrum have been reported by Bennett, Silver, and Ashley.[12] In addition, Madden, Canfield, and Hass[13] have obtained reflectance values in the vacuum ultraviolet region ultilizing a procedure which essentially eliminates the oxide problems that have affected previous work. These results have stimulated the present effort.

The purpose of the present paper is first to coordinate existing data for Al to yield a reflectance curve for the range between 0 and 22 eV, and to employ the Kramers-Kronig relation[14,15,9] to obtain the real and imaginary parts of the dielectric constants. These provide a complete description of the optical properties for this range. Secondly, we shall show that it is possible to achieve a rather complete degree of theoretical understanding of both the free electron and interband effects. In addition, because of the reliability of available band calculations, and the existence of some general sum rules involving these dielectric constants, it will be possible to isolate, at least partially, the many-body effects and estimate the degree to which they are likely to affect both the free electron and interband contributions.

The next section is concerned with a survey and analysis of existing reflectance data. The third section deals with an interpretation of the data. This section includes new information concerning the band structure and optical mass of Al and represents a continuation of the previously reported calculations by one of us (B.S.).[6]

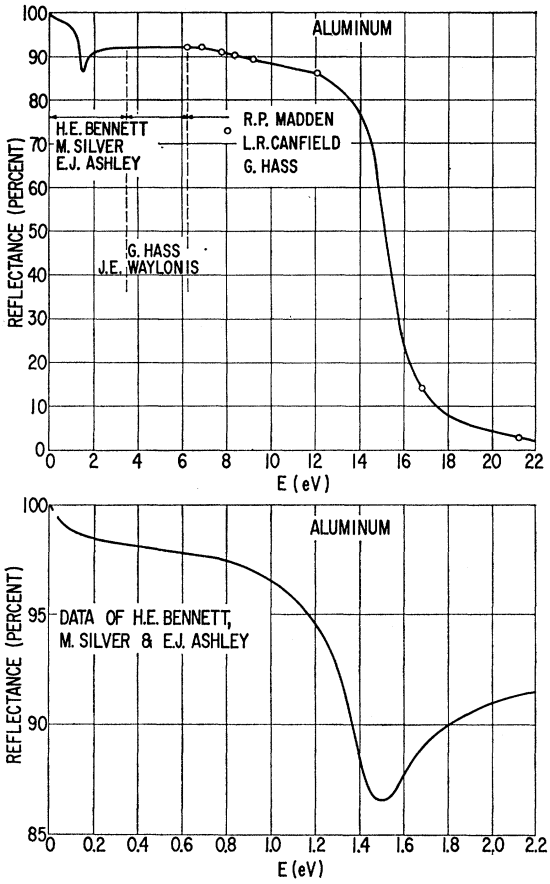

FIG. 1. The spectral dependence of the reflectance of Al. The curve is a composite of the data of Refs. 11, 12, and 13.

II. SURVEY AND ANALYSIS OF R DATA

Experimental work on the optical properties of Al has emphasized the spectral dependence of the reflectance.[11–13] Interest in this material stems primarily from its use as a mirror and as a comparison standard for reflectance measurements. Unfortunately, aluminum oxidizes quite rapidly upon exposure to air and results for exposed surfaces may be variable. This situation is most serious in the vacuum ultraviolet. A systematic study is being carried out by the U. S. Army Engineering Research and Development Laboratory and the U. S. Naval Research Laboratory on the optical properties of evaporated films in the extreme ultraviolet.[16] For carefully prepared aluminum surfaces, they[13] observe that the reflectance remains surprisingly high for quantum energies throughout the range to 12 eV provided the measurements are made quickly before appreciable exposure to even the relatively good vacuum of the monochromator. In addition, they are able to evaluate the optical constants at selected energies by performing experiments at various angles of incidence.

[10] L. G. Schulz, J. Opt. Soc. Am. 44, 357 (1954); L. G. Schulz and F. R. Tangherlini, J. Opt. Soc. Am. 44, 362 (1954).
[11] G. Hass and J. E. Waylonis, J. Opt. Soc. Am. **51**, 719 (1961) and cited references.
[12] H. E. Bennett, M. Silver, and E. J. Ashley, J. Opt. Soc. Am. **53**, 1089 (1963).
[13] R. P. Madden, L. R. Canfield, and G. Hass, J. Opt. Soc. Am. **53**, 620 (1963).
[14] F. C. Jahoda, Phys. Rev. **107**, 1261 (1957).
[15] H. R. Philipp and E. A. Taft, Phys. Rev. **113**, 1002 (1959).
[16] For a brief review of this work see G. Hass and W. R. Hunter, J. Quart. Spectr. Radiation Transfer **2**, 637 (1962).

TABLE I. A comparison of the results obtained in the present analysis with those of Schulz and Tangherlini and Hass and Waylonis for several values of E.

	6500 Å 1.91 eV			5500 Å 2.27 eV			4000 Å 3.10 eV		
	n	k	R (%)	n	k	R (%)	n	k	R (%)
Schulz and Tangherlini	1.24	6.60	89.8	0.76	5.32	90.3	0.40	3.92	90.8
Hass and Waylonis	1.30	7.11	90.7	0.82	5.99	91.6	0.40	4.46	92.7
Present analysis	1.55	7.70	90.6	0.99	6.60	91.7	0.51	4.83	92.0

At lower energy the effects of surface oxide are less serious. However, in this spectral region extremely small differences in reflectance are significant in evaluating and discussing the free-electron behavior of such materials. Thus, the environmental vacuum obtained during the preparation of specimens is important in that impurities may be introduced into the film in this process which can alter the optical parameters. Bennett, Silver, and Ashley[12] utilizing a precise measuring technique are able to distinguish their reflectance values obtained on samples prepared in ultrahigh vacuum (10^{-10} Torr) from those corresponding to conditions of high vacuum (10^{-6} Torr).

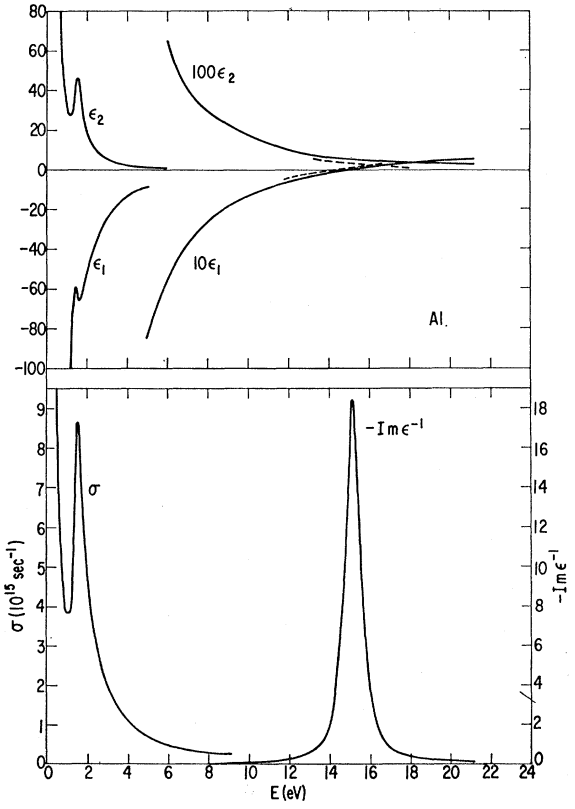

FIG. 2. The spectral dependence of the real and imaginary parts of the dielectric constant, the conductivity $\sigma=\omega\epsilon_2/4\pi$, and the energy loss function $-\mathrm{Im}\epsilon^{-1}$ for Al obtained by Kramers-Kronig analysis of the curve of Fig. 1. The results of LaVilla and Mendlowitz are shown by the dashed curves.

The curve of Fig. 1 represents a composite of what we believe to be the best data available for aluminum. Good agreement is found in the region of overlap of these measurements. The only arbitrariness in the figure lies in the manner in which the curve was drawn between the experimental points of Madden, Canfield, and Hass[13] for energies above 12.1 eV. The present curve was constructed such that the results of Kramers-Kronig analysis (1) gave a smooth curve for ϵ_1 and ϵ_2 in this region, (2) agreed with the n and k values of Ref. 13 at 16.87 eV and 21.2 eV, and (3) gave realistic values of the phase, θ, in the extrapolated region beyond 21.2 eV.[14,15,17]

Plots of the real and imaginary parts of the dielectric constant, ϵ_1 and ϵ_2, obtained by Kramers-Kronig analysis of the curve of Fig. 1 are shown in Fig. 2 along with values of the conductivity, $\sigma=\omega\epsilon_2/4\pi$, and the energy loss function, $-\mathrm{Im}\epsilon^{-1}$.

The optical constants obtained in the present study are higher than those of Schulz and Tangherlini[10] and of Hass and Waylonis.[11] This comparison is shown in Table I for several energies. An attempt was made to bring the results of the present analysis into better agreement with their values in the region of 1 to 3 eV, by adjustment of the curve above 21.2 eV. However, this could not be accomplished with any simple extrapolation of the reflectance which joined smoothly with the curve of Fig. 1 in addition to satisfying conditions (1) to (3) given above. It should be noted, however, that the results of the present analysis depend somewhat on the exact construction of the curve for R above 12.1 eV. Additional reflectance measurements to remove any remaining ambiguity are desirable.

The curve for $-\mathrm{Im}\epsilon^{-1}$, which is most strongly influenced by reflectance values above 12.1 eV, is in good agreement with the characteristic energy loss experiments of LaVilla and Mendlowitz[18] and of Powell and Swan[19] who observe peaks at 14.8 and 15.3 eV, respectively. The curve of Fig. 2 has its maximum near 15.2 eV. The comparison with LaVilla and Mendlowitz is indicated more explicitly by the dashed curves of

[17] The curve was linearly extrapolated in a plot of $\ln R^{\frac{1}{2}}$ versus $\ln E$ to 0.327% at 30 eV and to 1.349×10^{-3}% at 100 eV. The computed value of n at 30 eV is in good agreement with that of W. R. Hunter, J. Appl. Phys. **34**, 1565 (1963).

[18] R. LaVilla and H. Mendlowitz, Phys. Rev. Letters **9**, 149 (1962).

[19] C. J. Powell and J. B. Swan, Phys. Rev. **115**, 869 (1959).

Fig. 2 showing their values of ϵ_1 and ϵ_2 obtained by Kramers-Kronig analysis of energy loss data. Their results for ϵ_2 are relatively smaller, although the absolute difference is only about 0.02.

III. INTERPRETATION

The experimental results discussed in the preceding section may be analyzed along lines very similar to those used in previous work on Ag and Cu.[9] Since the longitudinal and transverse dielectric constants are equal in the long-wavelength limit and the photon wavelengths of interest here are all rather larger than the interatomic distance, we would expect to find the same plasma effects as those exhibited by characterisitc energy loss experiments, in addition to structure typical of optical intra- and interband effects. An expression for the complex frequency-dependent dielectric constants, $\epsilon(\omega)$, valid in the random-phase approximation, was discussed in Ref. 9. It was shown to be expressible in the form

$$\epsilon(\omega)=\epsilon^{(f)}(\omega)+\delta\epsilon^{(b)}(\omega), \tag{1}$$

which separated explicitly the intraband effects characteristic of free electrons,

$$\epsilon^{(f)}(\omega)=1-\omega_{pa}^2/\omega(\omega+i/\tau_c) \tag{2}$$

from the interband effects commonly associated with bound electrons,

$$\delta\epsilon^{(b)}(\omega)=-m^{-1}(e/\pi)^2\int d^3k\Sigma'_{ll'}f_l(\mathbf{k})f_{ll'}{}^{\mu}\,[(\omega+i/\tau_{ll'})^2-\omega_{ll'}{}^2]^{-1}. \tag{3}$$

The notation is the same as in Ref. 9: $\omega_{pa}=[4\pi ne^2/m_a]^{\frac{1}{2}}$ is the plasma frequency, n_c is the conduction electron density, m_a is the optical mass, the τ's are relaxation times associated with intra- and interband processes, $f_l(\mathbf{k})$ is the distribution function,

$$f_{ll'}{}^{\mu}=(2/\hbar\omega_{ll'}m)\,|P_{ll'}{}^{\mu}|^2$$

is the oscillator strength,

$$P_{ll'}{}^{\mu}=v_a{}^{-1}\int u_{l'}{}^*(k,x)p^{\mu}u_l(k,x)d^3x$$

being the momentum matrix element for direction μ integrated over the unit cell having volume v_a, and $\hbar\omega_{ll'}=E_l(\mathbf{k})-E_{l'}(\mathbf{k})$ the energy difference between bands l and l' at the point $\mathbf{k}$. Equation (2) is very similar to the well-known result of Drude for free electrons. Equation (3) resembles the Lorentz result for insulators. Interband transitions of conduction electrons are included in Eq. (3). For future application, it should be emphasized that each part of Eq. (1) satisfies the Kramers-Kronig relations.

The first task will be the separation of $\epsilon^{(f)}(\omega)$ from $\delta\epsilon^{(b)}(\omega)$. The discussion of Sec. F will show that our empirical separation, even though treated within the framework of the random-phase approximation, will be valid for an interacting many-electron system.

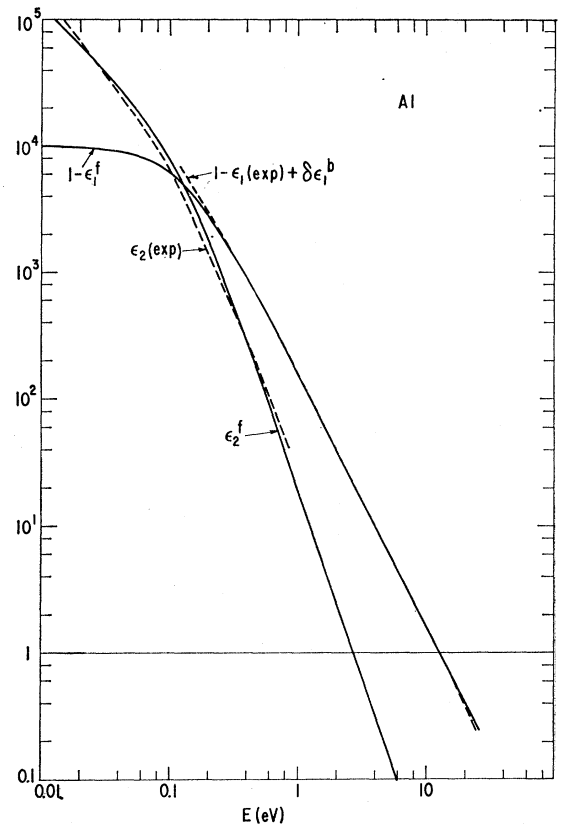

FIG. 3. Comparison of experimental and theoretical values of ϵ_1 and ϵ_2 for Al in the "free electron" range using Eq. (2) fitted to the experimental curve at 0.4 eV. The values of $\hbar\omega_{pa}$ and τ_c are found to be 12.7 eV and 5.12×10^{-15} sec, respectively. In order to utilize a logarithmic plot, the positive definite quantity $1-\epsilon_1{}^{(f)}$ is compared to $1-\epsilon_1(\exp)+\delta\epsilon_1{}^{(b)}$. The values of $\delta\epsilon_1{}^{(b)}$ are determined in Sec. B.

A. Free-Electron Effects

The separation of $\epsilon^{(f)}(\omega)$ from $\delta\epsilon^{(b)}(\omega)$ becomes possible if it is recognized that interband transitions do not set in until about $\frac{3}{4}$ eV, and that therefore it should be possible to fit the experimental results at lower energy to Eq. (2). In this range $\delta\epsilon_2{}^{(b)}=0$ and $\delta\epsilon_1{}^{(b)}$ is practically negligible compared to $-\omega_{pa}{}^2/\omega(\omega+i/\tau_c)$, the dominant term in ϵ_1. The results of fitting Eq. (2) to the experimental values of ϵ_1 and ϵ_2 at 0.4 eV are shown in Fig. 3. The corresponding values of $\hbar\omega_{pa}$ and τ_c are found to be 12.7 eV and 5.12×10^{-15} sec, respectively. In order to utilize a logarithmic plot, we have shown the positive definite quantity $1-\epsilon_1{}^{(f)}$ rather than $\epsilon_1{}^{(f)}$. This quantity is compared to $1-\epsilon_1(\exp)+\delta\epsilon_1{}^{(b)}$. The values of $\delta\epsilon_1{}^{(b)}$ are those to be determined in Sec. B. Clearly at 0.4 eV, $\delta\epsilon_1{}^{(b)}$ has negligible effect on the magnitude of ϵ_1. The agreement between the two sets of quantities is seen to be excellent over more than two decades. The

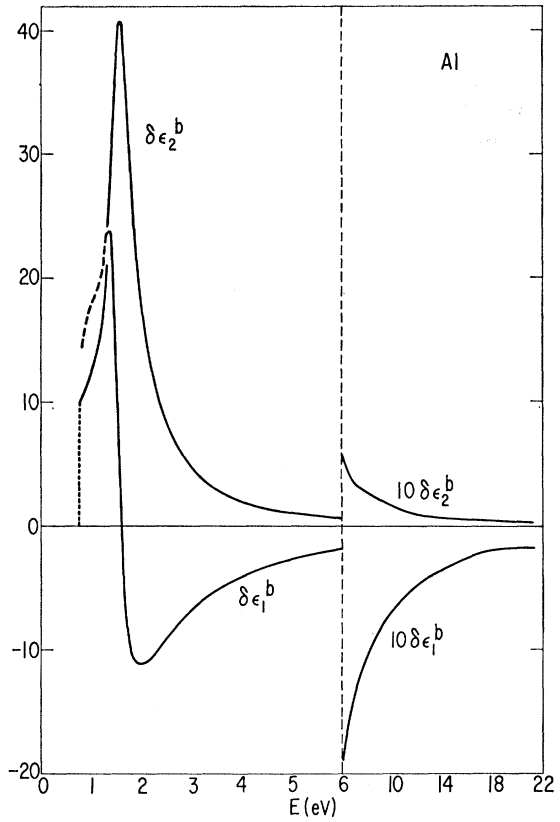

FIG. 4. The real and imaginary parts of $\delta\epsilon^{(b)}(\omega)$. The values of $\delta\epsilon_1{}^{(b)}$ are obtained by calculating $\delta\epsilon_2{}^{(b)}$ from $\epsilon_2(\text{exp})-\epsilon_2{}^{(f)}$ and using the Kramers-Kronig relation given in Eq. (4).

agreement in $1-\epsilon_1$ above 1 eV is a result of the construction of $\delta\epsilon_1{}^{(b)}$ from the Kramers-Kronig relation, as described in the next section and is not to be regarded as a test of the Drude formula. The disagreement for ϵ_1 at low energies (i.e., <0.1 eV), where ϵ_1 is strongly dependent on τ, may be due to several causes, e.g., an uncertainty in the film value for τ and its possible energy dependence.

The reasonableness of the magnitudes of ω_{pa} and τ_c can be ascertained in several ways. In Sec. E we shall discuss the plasma frequency obtained from the energy loss function $-\text{Im}\epsilon^{-1}$ around 15 eV and show it to be consistent with the data at low energies in an entirely different region of the spectrum. It is also possible to compute the magnitude of the dc conductivity $\sigma(0)=(1/4\pi)\omega_{pa}{}^2\tau_c$. We find $\sigma(0)=1.55\times10^{17}$ sec^{-1} in comparison to the experimental value 3.18×10^{17} sec^{-1} for bulk Al. That our result is a factor of 2 lower than the bulk value may be due to the fact that the measurements pertain to thin films, or alternatively that τ_c decreases rapidly from its dc value as the frequency is increased. From the extent of the agreement shown in Fig. 3, it is clear, however, that τ_c cannot be varying rapidly between 0.1 and 1 eV.

The value of the optical mass may be determined from ω_{pa} assuming there to be three free electrons per atom. We find $m_a=1.5$. Since the calculated energy bands are so free-electron-like it is clear that they would lead to a smaller m_a. We have estimated the optical mass, m_{ac}, predicted by band theory, by calculating the increments over the free-electron value produced by separate (111) and (200) Bragg reflectances associated with the previously determined pseudopotential.[20] The sum over 8 (111) and 6 (200) faces leads to a value of 1.2. In actuality, the effect of the planes cannot be separated, and the above procedure tends to overestimate the difference from the free-electron value. The 1.2 value is an upper limit with the proper value probably closer to 1.15. The discrepancy between the band structure value $m_{ac}=1.15$, and $m_a=1.5$ arises from the interactions neglected in the individual electron model. Since the electron-phonon interaction should be negligible at the energies of interest, the difference is attributed to many-electron effects, which will be discussed further in Sec. F. The magnitude of m_a is quite comparable to the thermal mass $m_t=1.6$ obtained from specific heat measurements.[21]

B. Separation into Intra- and Interband Parts

Since $\delta\epsilon_2{}^{(b)}=0$ in the region near zero frequency where ϵ_2 is largest, the separation into intra- and interband parts is most easily achieved by calculating $\delta\epsilon_2{}^{(b)}$ from $\epsilon_2(\text{exp})-\epsilon_2{}^{(f)}$ and then using the Kramers–Kroing relation

$$\delta\epsilon_1{}^{(b)}(\omega)=(\pi\omega)^{-1}\int_0^\infty \ln\left|\frac{(\omega+\omega')}{(\omega-\omega')}\right|\left(\frac{d}{d\omega'}\right)\times[\omega'\delta\epsilon_2{}^{(b)}(\omega')]d\omega' \quad (4)$$

to calculate $\delta\epsilon_1{}^{(b)}$. The advantage of this particular form lies in the fact that the machine program used to deduce the phase angle from the reflectance[15] may be immediately adapted to evaluate the integral in Eq. (4).

The subtraction used to obtain $\delta\epsilon_2{}^{(b)}$ should be quite accurate except in the vicinity where it first begins to rise from zero, since $\epsilon_2{}^{(f)}$ decreases quite rapidly with increasing frequency. In particular, it can be seen from Figs. 2 and 3 that $\epsilon_2{}^{(f)}$ contributes less than 20% to $\epsilon_2(\text{exp})$ above 1.5 eV. Thus, possible inaccuracies in $\epsilon_2{}^{(f)}$, as given by Eq. (2), due to a frequency dependence of τ_c should not be important. In the case of Ag, the separation was more clear cut, since interband transitions do not set in until nearly 4 eV, where $\epsilon_2{}^{(f)}$ is nearly zero.

The results for $\delta\epsilon_1{}^{(b)}$ and $\delta\epsilon_2{}^{(b)}$ are shown in Fig. 4. The imaginary part was truncated just below 1 eV in accord with the band calculations, since the contribu-

[20] The pseudopotential employed is given in Ref. 6. The procedures used in estimating m_{ac} and the density of states (in Sec. C) are similar to that given in F. S. Ham, Phys. Rev. **128**, 2524 (1962).

[21] D. H. Howling, E. Mendoza, and J. G. Zimmerman, Proc. Roy. Soc. (London) **A299**, 86 (1955).

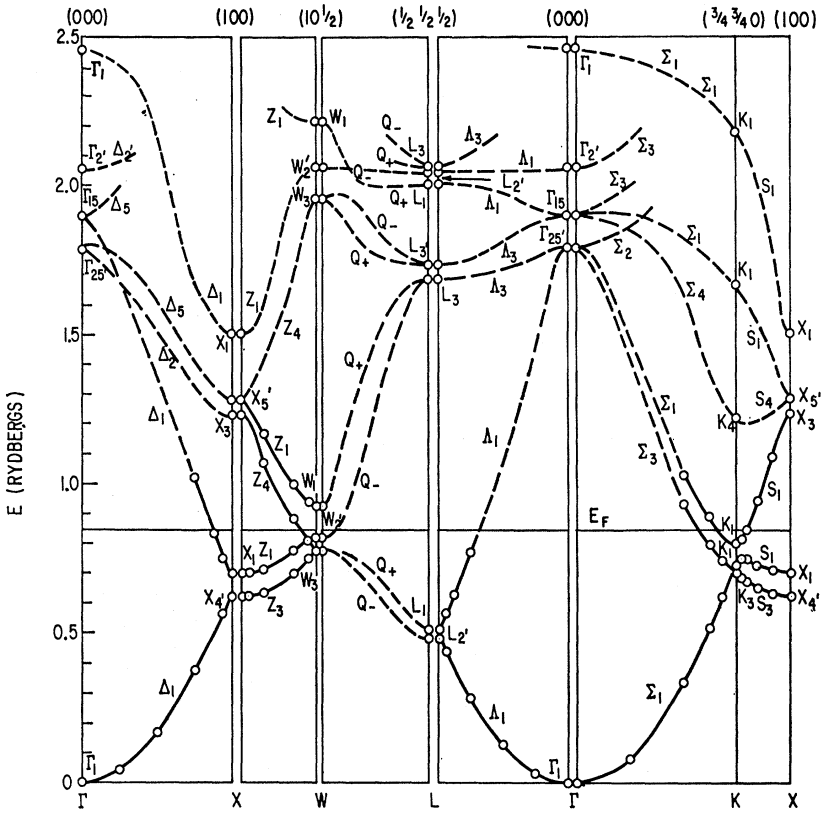

FIG. 5. The calculated energy bands of Al along the symmetry axes. The calculated values are given by the small circles. The dashed curves provide a rough indication of the bands between the widely spaced calculated values.

tion at lower energies may be due entirely to small inaccuracies in the Drude formula and/or the data analysis. Because of this inaccuracy, it was impossible to obtain meaningful values of $\delta\epsilon_1^{(b)}$ at lower frequencies. Above 1.5 eV, $\delta\epsilon_2^{(b)}$ should be quite accurate. A similar statement holds for $\delta\epsilon_1^{(b)}$ as obtained from Eq. (4).

The curves in Fig. 4 show quite clearly that the important interband transitions, giving rise to structure in $\delta\epsilon^{(b)}$, are confined to a small energy range surrounding 1.5 eV. The rapid decrease in magnitude of both dielectric constants at higher energies indicates that any futher interband transitions can make only a small contribution. In the next two sections, we shall identify the transitions responsible for the structure and present a semiquantitative theory which describes the shape of $\delta\epsilon_2^{(b)}$ reasonably well.

C. Interband Transitions

In order to understand the interband effects in detail, we will utilize the results of the energy band calculations for this metal. The energy bands for the various symmetry axes are shown in Fig. 5. The calculated values, which are indicated by the circles, are given relative to the s state at the center of the Brillouin zone (i.e., the Γ_1 level). The energy bands below roughly 1 Ry have been presented previously, while the higher energy symmetry point eigenvalues up to ≈ 2.4 Ry have been obtained for the present analysis. Aside from the lifting of the free-electron degeneracies and the elimination of crossings, the free-electron-like behavior noted previously for Al persists in the higher energy range.

In this and the following section, we will discuss the interband term, $\delta\epsilon_2^{(b)}$, in terms of the calculated energy band structure. Since $\delta\epsilon_1^{(b)}(\omega)$ can be obtained from $\delta\epsilon_2^{(b)}(\omega)$ by the Kramers-Kronig relations [e.g., Eq. (4)] it will not be considered separately. As can be seen directly from Eq. (3), the expression for $\delta\epsilon_2^{(b)}(\omega)$ in the limit of $\tau_{ll'} \rightarrow \infty$ is

$$\delta\epsilon_2^{(b)}(\omega) = e^2/(m^2\pi\hbar\omega^2)\int d^3k \; \Sigma_{l>l'} f_{l'}(\mathbf{k})|P_{ll'}{}^{\mu}|^2\delta(\omega-\omega_{ll'}). \quad (5)$$

The contribution for a given ω is then proportional to the joint density of states, $N_{ll'}(\omega) = (4\pi^3)^{-1}\int d^3k \times\delta(\omega-\omega_{ll'})$, times an average of $|P^{\mu}_{ll'}|^2$ over the surface $\omega_{ll'}(\mathbf{k})=\omega$. Structure in ϵ_2 is then expected to occur at critical points, i.e., where $\nabla_k\omega_{ll'}=0$. The critical points, in turn, generally occur at symmetry points where the gradients of $E_l(\mathbf{k})$ and $E_{l'}(\mathbf{k})$ may vanish separately due to symmetry.

The band calculations of Fig. 5 show that the only interband transitions below 8 eV at symmetry points are those between the two occupied p-like states $W_{2'}$ and W_3 and the unoccupied s-like state W_1. The calculated transition energies are 1.4 and 2.0 eV, respectively. It is

TABLE II. Estimated ratios of various interband contributions to the imaginary part of the dielectric constant.

Transition	Band gap (eV)	No. of valleys	Estimated averaged joint density of states ($a_0^{-3}\mathrm{Ry}^{-1}$)	Estimated ratios
$\left\{\begin{matrix}W_{2'}\rightarrow W_1\\ \Sigma_3\rightarrow\Sigma_1\end{matrix}\right\}$	1.41	$\begin{matrix}6\\12\end{matrix}$	2.3×10^{-3}	1
$W_2'\rightarrow W_1$	19.0	6	2.3×10^{-3}	0.008
$W_3\rightarrow W_1$	19.6	6	2.3×10^{-3}	0.008
$X_4'\rightarrow X_1$	12.0	3	4×10^{-4}	0.004
$X_1\rightarrow X_5'$	7.9	3	4×10^{-4}	0.008
$L_2'\rightarrow L_1$	20.7	4	3×10^{-4}	0.002
$L_2'\rightarrow L_3$	16.3	4	3×10^{-4}	0.003
$L_1\rightarrow L_3'$	16.6	4	3×10^{-4}	0.003
$\Gamma_1\rightarrow\Gamma_{15}$	25.1	1	5×10^{-3}	0.004

noteworthy that the lower energy transition coincides almost exactly with the position of the $\epsilon_2(\omega)$ peak, while the other falls in the trailing edge of the peak where ϵ_2 is still moderately high. It is quite clear then that the region around W must contribute significantly to the large peak in ϵ_2.

It might also be noted that interband transitions in the vicinity of the [110] (i.e., Σ) axis set in at about 1.4 eV. A detailed study of the $E(\mathbf{k})$ in this region shows that a critical point exists on the axis by virtue of the fact that the second and third band states below and above the Fermi level, respectively, are parallel there. These transitions thus also contribute appreciably to the 1.5 eV peak.

The energy band calculations predict that allowed higher energy transitions at symmetry points set in at about 8 eV and above. The experimental $\epsilon_2(\omega)$, however, exhibits no structure in this range.[22] To obtain a quantitative measure of the importance of the higher energy transitions at symmetry points,[23] we first note that the peak value of the contribution from a critical point is proportional to $E_g^{-3/2}$ where E_g is the energy gap [see, e.g., Eq. (6)]. In order to determine the relative importance of the various transitions, we will consider the product $\nu E_g^{-3/2}N_{ll'}(\omega)$, where ν is the number of valleys for the particular symmetry point. The factor $N_{ll'}(\omega)$ may be estimated using nearly free-electron-like behavior of the bands modified by the dominant Bragg reflection appropriate to the particular symmetry point.[24] To expedite these estimates, we have neglected the curvature of the upper band involved in the transition. The relevant factors and the estimated ratio with respect to the contributions from W and Σ are presented in Table II for the transitions below 20 eV and the 25 eV transition at Γ. It is evident that the higher energy transitions are much weaker than the 1.5 eV one, being at most about a percent of the latter. The principal reduction arises from the $E_g^{-3/2}$ factor, so that the numerous transitions at still higher energy would certainly be unimportant.

In the comparison, we have left out broadening effects which, of course, would be more serious for the higher energy transitions. We have also neglected the possible variation of the matrix element, P, with energy as this is difficult to estimate. Because of convergence requirements for the f-sum rule, P would be expected to decrease with increasing energy, thus reducing further the strength of the higher energy transitions.

The striking difference between Al and many monovalent metals, such as Cu, and Ag, deserves some comment. In these latter metals, structure due to interband transitions is observable in the high-energy range considered above. A comparison of the energy band structures of these metals shows that in contrast to Al the noble metals have $E(\mathbf{k})$ which deviate markedly from those of a free electron. The large splittings at symmetry points in the noble metals imply large effective masses. This and the large masses of the flat d bands reflect themselves in relatively more pronounced peaks in the joint density of states. The proximity of the noble metal d bands to the Fermi level allows for several additional interband transitions. In addition, there are arguments based on the sum rules which show that the transitions involving the d bands tend to be stronger at high energy.

The above comments are probably applicable, in a general way, to other polyvalent metals. That is, since they generally have rather free-electron-like band structures, the polyvalent metals will tend to have weaker short-wavelength interband transitions than the noble metals.

D. Low-Energy Transitions at W and Σ

In the previous section we suggested that the large sharp peak in ϵ_2 at about 1.5 eV is attributable to interband transitions from the regions around W and Σ. It was noted that the calculated values of the $W_1-W_{2'}$ and $\Sigma_1-\Sigma_3$ gaps agreed closely (i.e., to within 0.1 eV) with the position of the ϵ_2 peak while the W_1-W_3 gap is about 0.6 eV larger. While we believe the calculated energy separations for Al are sufficiently accurate to indicate the proper identification of the transitions, it is worthwhile to consider these transitions in more detail. A comparison of the shapes and magnitudes of

[22] There is some suggestion of structure in the reflectance curve (Ref. 13) near 10 eV. See W. R. Hunter, J. Opt. Soc. Am. (to be published). This detail could be evidence of interband transitions near this energy. As can be seen in Table II discussed below, the first set of interband symmetry point transitions are associated with critical points at X. The gaps are calculated to be about 8 and 12 eV.

[23] Consideration of interband band transitions was restricted to the symmetry points both because of the greater probability that they will occur at these points and for practical reasons. In regard to the latter, the $E(\mathbf{k})$ for the higher energy states were calculated only at the symmetry points. The likelihood of special circumstances leading to the flatness of $\hbar\omega_{ll'}(\mathbf{k})$, such as that at Σ(see Sec. D) is small.

[24] See Ref. 20.

the calculated contribution to $\delta\epsilon_2{}^b(\omega)$ from these regions with the experimentally obtained $\epsilon_2(\omega)$ would constitute an important check on the assignment. In addition, this investigation will provide us with an indication of how well the individual electron model, as given by the band calculations, describes the optical properties associated with interband transitions.

The simplest of these transitions to treat are those between the two bands which go into the degenerate W_3 level at the zone corner and the higher band associated with W_1. Except for some unessential complications, the relevant band differences, $\hbar\omega_{ll'}(\mathbf{k})$, form simple minima at W, and are adequately approximated for our purposes by the simple quadratic expressions $\hbar\omega(\mathbf{k})=E_g+\hbar^2/2m[(m/m_{\parallel})\Delta\mathbf{k}_{\parallel}{}^2+(m/m_{\perp})\Delta\mathbf{k}_{\perp}{}^2]$ where the symbols $\parallel$ and $\perp$ denote axes parallel and perpendicular to the X-W axis. The gap at W, E_g, has the value 2.0 eV, while $m/m_{\parallel}=7.5$ and $m/m_{\perp}=9.7$ for the transitions involving the higher W_3 band and $m/m_{\parallel}=25$ and $m/m_{\perp}=16$ for the lower band. It is clear that this case is analogous to the direct transitions from a maximum in the valence band of a semiconductor to a minimum in the conduction band. The contribution to the imaginary part of the dielectric constant is given by a simple generalization of Korovin's result.[25]

$$\delta\epsilon_2{}^b(\omega)=\gamma(\hbar\omega/E_g-1)^{\frac{1}{2}}(E_g/\hbar\omega)^2, \quad \hbar\omega>E_g,$$
$$=0, \quad \hbar\omega<E_g, \qquad (6)$$

with

$$\gamma=2\nu(e\hbar/m)^2|P_{ll'}|^2(m_{\parallel}/m)^{\frac{1}{2}}(m_{\perp}/m)(2m/\hbar^2E_g)^{3/2},$$

where $P_{ll'}$ is the average of the momentum matrix element over the surface $\omega_{ll'}(\mathbf{k})=\omega$.

The transitions between the $W_{2'}$ and W_1 bands are more difficult to compute because of the more complicated $\mathbf{k}$ dependence of the energy differences in this region. To illustrate this we note that for $\mathbf{k}$ along the W to X axes the energy difference is essentially a maximum at W. Similar behavior is found along the W to L axes which are mutually perpendicular and which lie in the plane through W, normal to the W-X direction. However, along another set of equivalent axes in this plane rotated from the previous set by 45°, the energy difference is a minimum at W. The gap $\hbar\omega_{ll'}(\mathbf{k})$ thus cannot be expressed as a simple quadratic function of $\Delta\mathbf{k}$. It must, in fact, be a nonanalytic function of $\Delta\mathbf{k}$, as a consequence of the near degeneracy of the p states. As a result of this complication, a numerical approach is required to determine the contribution to $\delta\epsilon_2{}^b(\omega)$ in the desired detail. Nevertheless, it is possible to see qualitatively that these transitions produce a peak. This follows from the fact that the Fermi level cuts off the transitions at energies slightly below and above the critical point just discussed.

In the previous section attention was called to the fact that the second (Σ_3) and third (Σ_1) bands about the [110] axes appeared to be quite parallel, and that these regions therefore could play an important role in producing the peak. The fact that the gap between the Σ_3 and Σ_1 bands arises from the splitting of degenerate free-electron bands along [110], suggests that insight into the nature of these levels can be obtained from consideration of the nearly free-electron picture. The nearly free-electron wave functions for $\mathbf{k}=2\pi a^{-1}(\kappa,\kappa,0)$ will be linear combinations of $\exp[i(\mathbf{k}+\mathbf{K}_n)\cdot\mathbf{r}]$, where the appropriate reciprocal vectors $\mathbf{K}_0$, $\mathbf{K}_1$, and $\mathbf{K}_2$ are given by $a(2\pi)^{-1}\mathbf{K}_n=0$, $(-1,-1,-1)$ and $(-1,-1,1)$. For the Σ_3 state the combination is

$$2^{-\frac{1}{2}}\{\exp[i(\mathbf{k}+\mathbf{K}_1)\cdot\mathbf{r}]-\exp[i(\mathbf{k}+\mathbf{K}_2)\cdot\mathbf{r}]\}$$

and the energy

$$E(\Sigma_3)=(m/m^*)(2\pi/a)^2[1+2(\kappa-1)^2]-V(2,0,0)$$

where $V(\mathbf{K}_n)$ is the Fourier component of the pseudopotential. The Σ_1 state is a linear combination of $\exp[i\mathbf{k}\cdot\mathbf{r}]$ and $\{\exp[i(\mathbf{k}+\mathbf{K}_1)\cdot\mathbf{r}]+\exp[i(\mathbf{k}+\mathbf{K}_2)\cdot\mathbf{r}]\}$, and it can be shown simply that with the neglect of a second-order term in the small quantity, $V(111)$, the energy is $E(\Sigma_3)+2V(200)$. Thus, in this approximation, which has been shown to be quite good for Al,[6] the energy difference along Σ is nearly a constant with a value of $2V(200)$. The argument is easily extended to show that the corresponding energy difference for $\mathbf{k}$ off the axis but in the (100) plane containing it is also rather constant. For $\mathbf{k}$ with components perpendicular to the (100) plane, however, the gaps will change due to the mixing of the states. From the above and from the fact that there are 12 Σ axes, it is apparent that the transitions from these regions make a large contribution to the ϵ_2 peak.

The numerical evaluation of $\delta\epsilon_2{}^b$ involves the computation of the joint density of states satisfying the proper occupancy conditions. In general it is difficult to determine a density of states with reasonably good resolution because of the very large number of $\mathbf{k}$ at which the eigenvalues $E_n(\mathbf{k})$ are required. In this case the task is feasible because of the reasonably small regions of the zone to which the contributions are localized. Also, the work is greatly simplified by the applicability of the pseudopotential method to Al. The computations were carried out by calculating the energies and energy differences on a relatively fine three-dimensional mesh, corresponding to roughly 10^6 points for the complete zone. A histogram for the joint density of states was obtained by counting the number of points having the appropriately occupied states and having $\hbar\omega_{ll'}$ in a given interval. A smooth curve was fitted to the histogram.[26]

The contribution from the neighborhood of W was

[25] L. I. Korovin, Fiz. Tverd. Tela **1**, 1311 (1959) [translation: Soviet Phys.—Solid State **1**, 1202 (1960)].

[26] Similar calculations have recently been carried out by D. Brust, J. C. Phillips, and F. Bassani, Phys. Rev. Letters **9**, 94 (1962) for Ge and by D. Brust, M. L. Cohen, and J. C. Phillips, Phys. Rev. Letters **9**, 389 (1962) for Si.

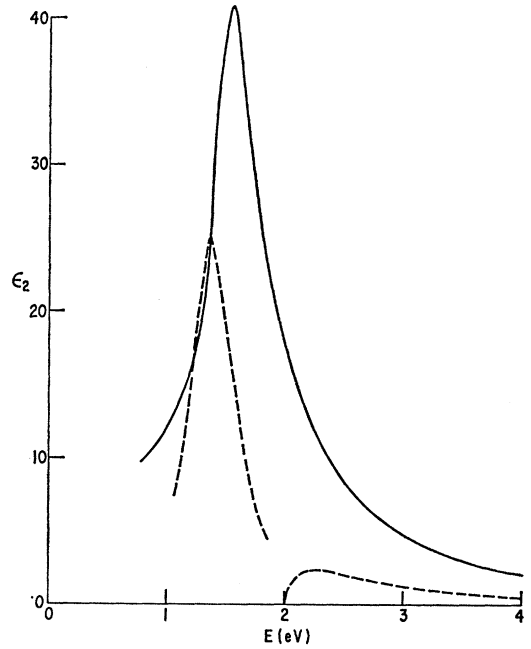

FIG. 6. The calculated contributions to the imaginary part of the dielectric constant from the interband transitions around W and Σ. The dashed peak is the sum of the contributions from the transitions between the $W_{2'}$ and W_1 bands and between the Σ_3 and Σ_1 bands. The dashed curved starting at 2.0 eV is associated with the transition from the W_3 bands to the W_1 band. For comparison purposes, the experimentally determined interband part of $\epsilon_2(\omega)$ is given by the solid curve.

found to lead to a sharp peak as expected. Since the contributing regions do not extend far from W in any direction, the approximation of using the value of $|P_{ll'}|^2$ evaluated at W appears justifiable. For the Σ regions, however, it was found that the energy differences are nearly constant over appreciable distances in each (001) plane in accord with the discussion above. The assumption of a constant matrix element is then probably poor. In particular, for the (001) plane containing the Σ axes, the gap under discussion is simply connected with that between the $W_{2'}$ and upper W_3 band. At W, $|P|^2$ is expected to be quite small because of the large p character of the $W_{2'}$ and W_3 states. To avoid the very laborious task of determining a large number of momentum matrix elements, we have assumed P to vary linearly from a fixed value on the (110) plane containing the Σ axis to zero in a distance corresponding to that between K and W. This approximation, which probably leads to an underestimate of the magnitude, does not appreciably affect the shape which is quite similar to the peak due to the transitions around W.

The momentum matrix elements for the transitions $W_{2'}$ to W_1 and Σ_3 to Σ_1 at the approximate center of the allowed range [i.e., $\mathbf{k}=2\pi a^{-1}(5/8,5/8,0)$] were evaluated using the wave functions inside and outside the inscribed sphere determined by the procedures described in Ref. 6. The resulting values of $E_p=2|P|^2/m$ are 0.65 and 0.48 Ry, respectively. With these values and the free-electron value for E_F, the contribution for the Σ transitions is found to be about 50% larger than that from the W region. The latter is affected moderately by a shift in E_F while the former is relatively insensitive to it since the changes in the occupancy of the Σ_3 and Σ_1 bands have compensating effects. The resulting $\delta\epsilon_2{}^b(\omega)$ is shown in Fig. 6 as the dashed peak between 1 and 2 eV.

In evaluating the contribution of the W_3 to W_1 band transitions to $\delta\epsilon_2{}^b$, we note that we will be concerned with energies well above the gap at 2.0 eV. At these energies there will be an increasing admixture of p and s components in the W_1 and W_3 bands, respectively. This leads to an energy-dependent reduction in E_p which is calculated to be 0.72 Ry at W. The effect was estimated by determining the variation for a few points along the $\|$ (or Z) and $\perp$ axes and by taking the arithmetic average. The result, with its characteristic "edge" shape, is shown in Fig. 6 as the dashed curve above 2 eV.

It is clear that aside from the dimple at 2 eV, the shape of the calculated $\delta\epsilon_2{}^b$ is entirely similar to that obtained from experiment. The magnitude, on the other hand, is significantly less. The deviation could be due, at least in part, to inadequacies in the computational procedures. It could also be due to many-electron effects as will be discussed below .

Since the interband effects depend upon the Fermi level, it might appear that this study could shed some light on the unsettled question of the position of the Fermi level relative to the p states at W. However, due to the substantial contribution from the Σ_3 to Σ_1 transitions and its relative insensitivity to changes in E_F, no conclusions concerning this important point are possible.

E. Plasma Effects

We now turn to a discussion of the dielectric constants at higher energies. The outstanding feature in this range is the strong and sharp peak in the energy loss function $-\mathrm{Im}\epsilon^{-1}$ at 15.2 eV. This energy is generally associated with the plasma resonance. In the present context, we must show that this value is consistent with the result $\hbar\omega_{pa}=12.7$ eV obtained in the low-frequency range where free-electron effects predominate.

In the far infrared ϵ is determined by $-\omega_{pa}{}^2/\omega(\omega+i/\tau_c)$, the contribution of $1+\delta\epsilon^{(b)}$ being relatively unimportant. Near the plasma resonance, $\hbar\omega_p$, at about 15 eV, ϵ_2 is very small so that ω_p is determined quite accurately by the condition that $\epsilon_1(\omega_p)=0$. This implies that

$$1-\omega_{pa}{}^2/\omega_p{}^2+\delta\epsilon_1{}^{(b)}(\omega_p)=0, \qquad (7)$$

since $\omega\tau\gg1$, and hence that $\omega_p=\omega_{pa}/[1+\delta\epsilon_1{}^{(b)}(\omega_p)]^{\frac{1}{2}}$. The contribution of $\delta\epsilon_1{}^{(b)}$, whose value is about -0.3, is therefore quite important in determining the magnitude of ω_p. We may determine a self-consistent solution of Eq. (7) using the preceding value of ω_{pa} and $\delta\epsilon_1{}^{(b)}$ as

given in Fig. 4. We find $\hbar\omega_p = 15.2$ eV, in agreement with the location of the peak in the energy loss function. The fact that ω_p is greater than ω_{pa} results from the negative value of $\delta\epsilon_1^{(b)}$ which is a remnant of the oscillator-like dispersion associated with the interband transitions near 1.5 eV.

Since the oscillator strength for the valence band is essentially exhausted in this region and transitions from the L shell do not set in until about 70 eV, the dielectric constant should be well approximated by its general asymptotic form[27] $\epsilon(\omega) = 1 - 4\pi ne^2/m\omega^2$, where m is the free-electron mass and n corresponds to 3 valence electrons per atom. Thus, the plasma frequency can be written alternatively in the form $\omega_p = [4\pi ne^2/m]^{\frac{1}{2}}$. Direct substitution into the preceding expression yields $\hbar\omega_p = 15.8$ eV, in good agreement with our earlier result of 15.2 eV. The neagtive value of $\delta\epsilon_1^{(b)}$ is therefore seen to raise the value of the plasma frequency from its lower value ω_{pa}, as determined by the optical effective mass, nearly to the larger value $[4\pi ne^2/m]^{\frac{1}{2}}$ required by the correct asymptotic behavior.

The extent of the agreement among these independent experimental and theoretical determinations of the plasma frequency indicates the consistency of our results, and, in particular of the determination of ω_{pa} and $\delta\epsilon_1^{(b)}$ from the low-energy data.

F. Sum Rules and Many-Electron Effects

The sum rules

$$\int_0^\infty \omega\epsilon_2(\omega)d\omega = \tfrac{1}{2}\pi\omega_p^2, \tag{8}$$

$$-\int_0^\infty \omega \mathrm{Im}\epsilon^{-1}(\omega)d\omega = \tfrac{1}{2}\pi\omega_p^2, \tag{9}$$

are exact for the interacting many-electron system.[28] Here $\omega_p^2 = 4\pi ne^2/m$, n is the total electron concentration, and m the free-electron mass. The numerical evaluation of the integrals from the experimental data therefore includes the effects of electron interactions among the valence electrons. As noted above, the core states of Al are sufficiently far removed ($\sim$70 eV) from the $3s$ and $3p$ electrons; it is thus possible to neglect them in the application of the preceding sum rules to the optical properties over the range considered here. We therefore expect that the above integrals should saturate at values of $\frac{1}{2}\pi\omega_p^2$ corresponding to three electrons per atom.

As in the previous work on Ag and Cu, it is useful to define the integrals of Eqs. (8) and (9) for a finite range in terms of an effective number of electrons, n_{eff} contributing to the optical properties over this range. Thus,

$$\int_0^{\omega_0} \omega\epsilon_2 d\omega = \tfrac{1}{2}\pi\left(\frac{4\pi e^2}{m}\right) n_{\mathrm{eff}}(\omega_0), \tag{10}$$

and similarly for the sum rule involving $\mathrm{Im}\epsilon^{-1}(\omega)$.

[27] P. Nozières and D. Pines, Nuovo Cimento **9**, 470 (1958).
[28] P. Nozières and D. Pines, Phys. Rev. **113**, 1254 (1959).

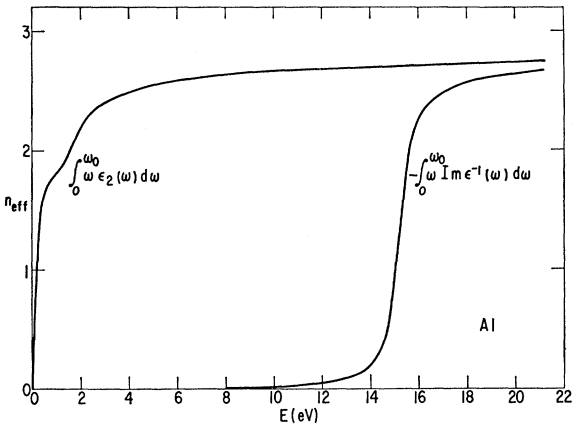

FIG. 7. The effective number of electrons per atom versus E obtained from numerical integration of experimental ϵ_2 and $-\mathrm{Im}\epsilon^{-1}$. The n_{eff} are defined by Eq. (10) and the corresponding analog of the sum rule for $-\mathrm{Im}\epsilon^{-1}$.

Figure 7 shows a plot of n_{eff} versus $E = \hbar\omega_0$ obtained from a numerical evaluation of the two integrals using the experimental data. The rapid initial rise in n_{eff} corresponding to Eq. (10) is due to free-electron effects which, in the absence of interband transitions, would produce saturation at a value of n_{eff} such that $4\pi n_{\mathrm{eff}}e^2/m = \omega_{pa}^2$. The break in the curve near 1.5 eV arises from the strong interband transitions at W and Σ discussed in Sec. D. The fact that the curve rises rapidly and reaches a value 2.7 near 22 eV, indicates that the f-sum rule for all $\mathbf{k}$ in the Brillouin zone is essentially exhausted.[29] Its shape is quite consistent with the fact, discussed in Sec. C, that the transitions near 1.5 eV at W and Σ are the only strong ones involving the valence electrons.

The n_{eff} plot corresponding to the other sum rule begins to increase only when the energy loss function becomes large. It is also seen to saturate at a value near 3, indicating that the entire energy loss is concentrated in a very small energy region about the plasma resonance. This fact, of course, is closely related to the absence of strong interband transitions at higher energies, and the concomitant reduction in the value of ϵ_2.

The simplicity of the preceding results is remarkable when it is contrasted with the corresponding situation in d-band metals[9] or semiconductors.[30] In the latter cases interband transitions involving the valence electrons persist to rather high energies, and empirical evaluation of the sum rules do not yield values of n_{eff} anywhere near saturation.

Even when the electron-electron interactions are taken into account, the wave functions in a solid are

[29] An extension of the studies to higher energy by one of us [H. R. Philipp (to be published)] shows that the integral for n_{eff} continues to rise in the region beyond 20 eV and reaches the value 3.0 electrons per atom just below the L-absorption edge at 70 eV.
[30] H. R. Philipp and H. Ehrenreich, Phys. Rev. **129**, 1550 (1963).

still labeled by band index n and wave number $\mathbf{k}$. Thus, it is possible, in the long-wavelength limit, to make a general separation into intra- and interband contributions as indicated in Eq. (1). The sum rule given by Eq. (8) may therefore be written as

$$\int_0^\infty \omega\epsilon_2^{(f)}(\omega)d\omega+\int_0^\infty \omega\delta\epsilon_2^{(b)}(\omega)d\omega=\tfrac{1}{2}\pi\omega_p^2. \quad (11)$$

Silin[31] has shown that a relationship of the form of Eq. (2) is still valid for a Fermi liquid below the onset of interband transitions provided that $\omega\tau_c>1$. The constants ω_{pa} and τ_c, however, now involve the function $\Phi(\mathbf{p},\mathbf{p}')$, describing the correlation among the particles, as well as the quasiparticle energy. Silin describes their effect on ϵ_1 by replacing the n in ω_{pa} by an effective number of particles, a procedure which we have also adopted in Fig. 7. For the present purposes, it is more convenient to think of a modified optical mass m_a^* while retaining the number of electrons as three per atom. It should be noted that the "dressing" effect which changes m_{ac} to m_a would vanish according to Landau's effective mass theorem[32] if the system were translationally invariant. In the range $\omega\tau_c>1$, the dressing is therefore a direct consequence of the periodic lattice.

The preceding discussion shows that the empirical separation of ϵ into intra- and interband effects made in Sec. B should be generally valid, since all that was used to accomplish it was the frequency dependence of $\epsilon_1^{(f)}$ and $\epsilon_2^{(f)}$ in the range $\omega\tau_c>1$. In order to fit $\epsilon_1(\omega)$, which is essentially independent of τ_c in this range, it was necessary to assume $m_a=1.5$ in contrast to the results from band theory (cf. Sec. A), which yielded $m_{ac}\cong 1.15$. The difference is attributed to many-electron effects, which are seen to increase the effective mass. The discussion of plasma effects in Sec. E is then also seen to be valid within this more general framework.

The sum rule given by Eq. (11) shows that many-electron effects will *decrease* the contribution of the intraband terms, and correspondingly *increase* that of the interband terms.

With the values of m_{ac} and m_a at hand, it is possible to estimate very roughly how much the calculation of the bound parts of the dielectric constants arising from the important interband transitions at W and Σ should be in error due to the neglect of many-electron effects.

We define $I_c=\int_0^\infty \omega\delta\epsilon_2^{(b)}$ (calc.)$d\omega$, where $\delta\epsilon_2^{(b)}$ (calc.) is the function calculated in Sec. D, and correspondingly I_e involving the experimental values of $\delta\epsilon_2^{(b)}$. Then the effect of the electron-electron interactions can be expressed in terms of the ratio I_e/I_c. Noting that from Eq. (2), $\int_0^\infty \omega\epsilon_2^{(f)}d\omega=(\frac{1}{2})\pi\omega_{pac}^2$ or $(\frac{1}{2})\pi\omega_{pa}^2$ if we are speaking, respectively, of undressed or dressed particles characterized, respectively, by m_{ac} and m_a, we have

$$\begin{aligned} I_e/I_c&=(\omega_p^2-\omega_{pa}^2)/(\omega_p^2-\omega_{pac}^2)\\ &=(m^{-1}-m_a^{-1})/(m^{-1}-m_{ac}^{-1}). \end{aligned} \quad (12)$$

Since ω_p and ω_{pac} are quite comparable in magnitude, the value of I_e/I_c depends fairly sensitively on the calculated m_{ac}. For the best value ($m_{ac}=1.15$), $I_e/I_c=2.6$, whereas for $m_{ac}=1.2$, $I_e/I_c=2.0$. A numerical integration of $\delta\epsilon_2^{(b)}$ (calc.) as determined in Sec. D yields $I_e/I_c\cong 3$, a value which is reasonably consistent with the calculated optical mass. Many-electron effects are thus seen to affect not only the mass at the Fermi surface, but also the strength of interband transitions.

ACKNOWLEDGMENTS

The authors are very grateful to Dr. Bennett, Dr. Silver, and Dr. Ashley for a copy of their manuscript in advance of publication. They also wish to thank Miss Elise Kreiger and Miss Doris Olechna for their capable help in obtaining the numerical results reported in this paper.

[31] V. P. Silin, Zh. Eksperim. i Teor. Fiz. **34**, 70 (1958) [translation: Soviet Phys.—JETP **7**, 486 (1958)].

[32] L. Landau, Zh. Eksperim. i Teor. Fiz. **36**, 1058 (1956) [translation: Soviet Phys.—JETP **3**, 920 (1957)].